Journal of Materials Chemistry C

ROYAL SOCIETY OF CHEMISTRY

PAPER

View Article Online
View Journal | View Issue

Cite this: J. Mater. Chem. C, 2025, 13, 23107

Oxygen incorporation in $YBa_2Cu_3O_{7-\delta}$ thin films: surface activation and degradation

Alexander Stangl,*[ab] Xavier Obradors,[b] Anna Palau,[b] Arnaud Badel[ac] and Teresa Puig*[b]

The oxygen off-stoichiometry plays a pivotal role for the physical properties of superconducting oxides. Yet, there is a lack of knowledge on the fundamental processes of oxygen incorporation and correlated phenomena during oxygen post annealing treatments. Here, we deployed electrical probes ($\rho(T)$ and electrical conductivity relaxation (ECR) measurements) to gain a better understanding of the kinetics of the oxygen reduction reaction (ORR) in epitaxial $YBa_2Cu_3O_{7-\delta}$ (YBCO) thin films. We identified a new indicator for the onset temperature of oxygen incorporation and report for the first time drastic kinetic deactivation in bare YBCO. We demonstrate that surface decoration using silver micro islands both catalytically activates oxygen incorporation and bypasses surface degradation processes. Our results suggest that the ORR in the studied YBCO samples is limited by a surface reaction. Additionally, weak XRD signatures of the formation of extended bulk defects were identified, which have to be considered in the designing of an optimal oxygenation treatment to obtain best performing superconducting YBCO.

Received 8th August 2025,
Accepted 16th October 2025

DOI: 10.1039/d5tc02998h

rsc.li/materials-c

1. Introduction

Oxide materials are considered game changers in the pursuit for a sustainable energy transition, due to their promising potential in the domains of energy harvesting, conversion, transport and storage, including oxide photovoltaics,[1,2] solid oxide fuel and electrolysis cells (SOFC & SOEC),[3,4] fusion-enabling high temperature superconductors (HTS),[5–8] and novel oxygen ion batteries.[9,10] For many members of this functional oxides materials class, the flexible oxygen off-stoichiometry, δ, is vital to their physical properties.[11–13] This is especially true for superconducting oxides, such as $YBa_2Cu_3O_{7-\delta}$ (YBCO), where δ does not only govern the structural transition to the superconducting orthorhombic phase,[14] but also determines the superconducting critical temperature, T_c,[15] and strongly impacts the maximum critical current density, J_c,[16–20] *via* the release of electronic charges (charge doping) to the crystal upon oxidation. Thus, precise control of the oxygen stoichiometry is a pivotal step in the manufacturing of high performing superconducting materials, including so called coated conductors,[21] which represent the commercial solution to the strict crystallographic requirements to unfold the full current carrying capacity of ReBCO (Re = rare earths, such as Y, Gd, Eu) materials.

Significant progress in understanding oxygen incorporation processes and identifying influencing factors has been made in the field of solid oxide cells, where the oxygen reduction reaction (ORR) is at the heart of operation.[22–25] The ORR, describing the incorporation of an oxygen molecule into crystal sites, $O_O^\times$, can be simply written as:†

$$O_{2,gas} + 2v_O^{\bullet\bullet} \rightleftharpoons 2O_O^\times + 4h^\bullet \quad (1)$$

with the oxygen vacancy, $v_O^{\bullet\bullet}$, and positively charge electron holes, $h^\bullet$. Nevertheless, it consists of a succession of elementary reaction steps, including adsorption, ionization, dissociation, recombination, surface and bulk diffusion of different charged oxygen species as well as electronic charges, as schematically illustrated in Fig. 1(a). Consequently, such interfacial, combined electronic and ionic charge transfer reactions are highly complex. Challenging, but progressively systematic studies deploying novel approaches and tools,[22,26,27] strive to illuminate the reaction pathways and identify the slowest elementary mechanism in the chain of reaction steps, thus the rate determining step (RDS), with the goal to improve the performance of catalysts, as well as of oxide electrodes and provide better control in tuning functional properties of mixed ionic electronic conductors (MIECs).

Based on sample dimensions and materials properties, one can distinguish two limiting cases for oxygen incorporation:

[a] CNRS, Grenoble INP, Institut Néel, Université Grenoble Alpes, 38000 Grenoble, France. E-mail: alexander.stangl@neel.cnrs.fr
[b] Institut de Ciència de Materials de Barcelona (ICMAB-CSIC), 08193 Bellaterra, Barcelona, Spain. E-mail: teresa.puig@icmab.es
[c] CNRS, Grenoble INP, G2ELab – Institut Néel, Université Grenoble Alpes, 38000 Grenoble, France

† Charges are indicated following the Kröger–Vink notation, with × and • corresponding to neutral and positive charge, respectively, relative to the perfect, defect-free crystal.

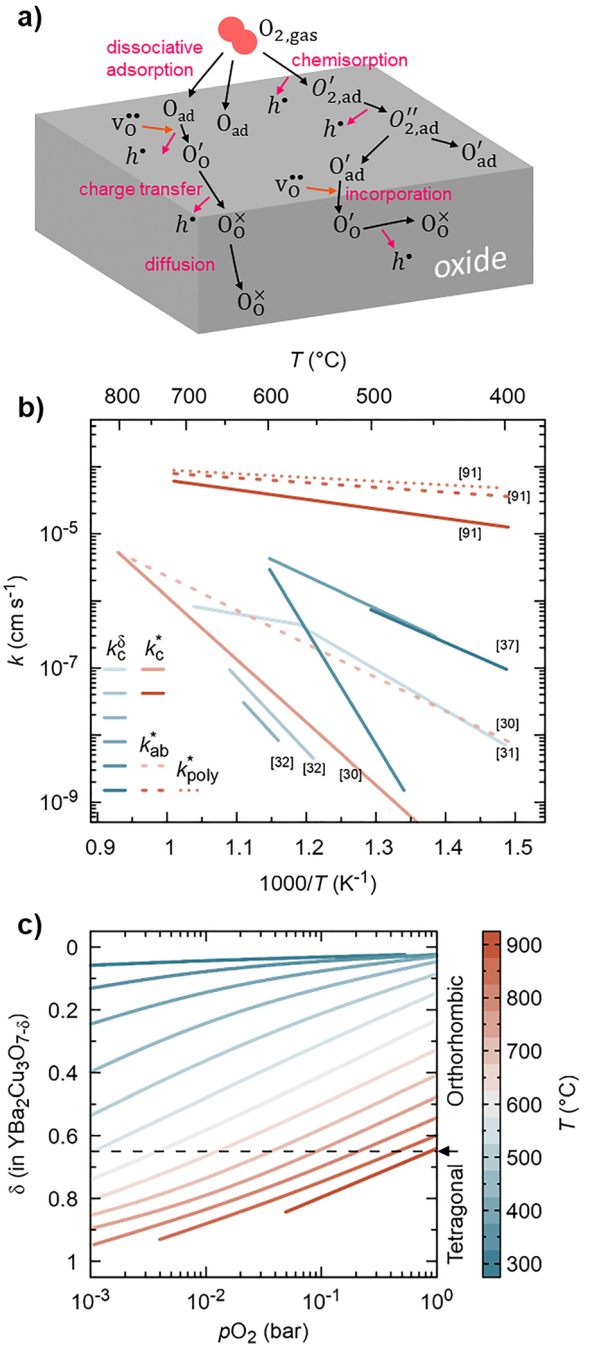

Fig. 1 (a) Sketch showing different reaction pathways for the process of oxygen incorporation into an oxide, including various elementary reaction steps, such as adsorption, ionization, dissociation, incorporation and diffusion, involving different defect species such as adsorbed (ad) and incorporated oxygen ions (O_{ad}, O'_O, $O^{\times}_O$, *etc.*), oxygen vacancies ($v^{\bullet\bullet}_O$) and electron holes ($h^{\bullet}$), given in Kröger–Vink notation. Notably, a large number of other reaction pathways are similarly possible. (b) Comparison of reported k values obtained *via* tracer experiments (k^*, red) and chemical experiments ($k^{\delta} = k_{chem}$, blue) for different crystal directions (solid/dashed lines for surface terminations normal/parallel to the c-axis, dotted line for polycrystalline sample).[91] (c) Oxygen off-stoichiometry, δ, of bulk $YBa_2Cu_3O_{7-\delta}$ as function of pO_2 at various temperatures, adapted from literature.[49]

bulk diffusion and surface exchange limitation.[28] For thin films of thickness d_{film}, oxygen incorporation can be reduced to a 1D problem (along the out-of-plane direction) and one can introduce the dimensionless parameter L, also referred to as Biot number:

$$L = \frac{d_{film} k_{chem}}{D_{chem}} \quad (2)$$

with the surface exchange and bulk diffusion coefficients, k_{chem} and D_{chem}, respectively. For $L \ll 1$, any oxygen concentration gradient along the thickness vanishes and the materials response to changes in the oxygen chemical potential (*e.g.* due to changes in the surrounding oxygen partial pressure) is determined by the surface only (surface exchange limited regime). Conversely, for $L \gg 1$, the top surface layer rapidly equilibrates to a new pO_2 in the atmosphere, while a concentration profile develops as function of distance to the surface (diffusion limited regime).

As for the YBCO community, which started historically with the analysis of bulk materials, the spotlight was focused for a long time on oxygen diffusion,[29–34] with little consideration of the importance of surface reactions.[35] While this remains plausible for bulk with large diffusion lengths or low density,[36] highly porous materials, the emergence of highly dense, low porosity thin films, as required for superconducting applications, calls for a revision of this picture. In particular, we suggested recently,[37] that oxygen incorporation in YBCO thin films may be exclusively governed by surface reactions, such as ionisation, dissociation and/or recombination of an oxygen surface ion with a bulk vacancy. This is in agreement with other recent reports on YBCO,[38] and a large number of similar thin film perovskite-related oxide materials, where the RDS was identified to rest within the surface,[39–44] and supported by previously reported fast grain-boundary assisted diffusion in YBCO.[45] Generalizing these results however, is problematic, as it may be very much dependent on the specific YBCO specimen. Namely, the materials chemistry itself can strongly depend on the sample type (bulk, powder, thin film), structure (single crystal, polycrystalline, epitaxial) and derived properties, such as density, porosity, surface termination and surface chemistry, number and type of bulk and surface defects and may strongly be affected by the synthesis technique. This results in a wide spread of reported surface exchange coefficients for different YBCO materials, spanning several orders of magnitude, as summarized in Fig. 1(b). Other effects however, including surface contamination, catalytic surface activation and detrimental deactivation, have been addressed insufficiently for ReBCO materials, leading to a materials history component which needs to be considered[46–48] and will be subject of this work.

While the above discussed phenomena are of kinetic nature, the equilibrium oxygen stoichiometry in an oxide is defined thermodynamically *via* its oxygen chemical potential and is as such a function of oxygen partial pressure as well as temperature, with inverse effects on the oxygen concentration.[50] That means increasing the pO_2 leads to a higher oxygen stoichiometry, while higher temperatures increase the configurational entropy and thus result in a lower overall oxygen concentration, due to a higher number of point defects, such as oxygen

vacancies. An oxygen non-stoichiometry diagram for bulk YBCO adapted from literature,[49] is shown in Fig. 1(c). As superconducting properties improve with increasing oxygen content, low annealing temperatures are favourable to obtain $\delta \approx 0$. However, the kinetic process of oxygen incorporation is thermally activated, resulting in a trade-off conflict between fast kinetics at high T and a small off-stoichiometry a low T. It may therefore seem beneficial to start the oxygenation process at high temperatures, where oxygen vacancies are rapidly filled and subsequently decrease the temperature to slowly occupy the remaining vacant oxygen sites. In fact, a similar process may be followed by some commercial coated conductor tape manufacturers.[33,51] However, this intuitive approach omits possible degradation processes, such as surface poisoning, morphological reconstruction, formation of extended bulk defects, *etc.*, which are commonly observed in oxide electrodes for high temperature applications (SOFC, SOEC),[52–56] as well as HTS materials[57] and can result in strongly reduced reaction rates, making processes slow and ineffective. Consequently, these processes have to be considered in designing an optimized oxygenation process.

Here, we use electrical conductivity relaxation (ECR) measurements to study the oxygen activity of bare and Ag decorated YBCO thin films as function of temperature and history, completed by a microstructural analysis. We investigate for kinetic degradation in bare YBCO, catalytic activation phenomena induced by silver coating and develop a possible, yet simplified reaction pathway scenario of oxygen kinetics in YBCO, with the goal to provide guidelines for improved oxygenation treatments.

2. Experimental

Thin films studied within this work were synthesized using the chemical solution deposition (CSD) technique,[58] whereas anhydrous TFA precursor salts were dissolved in trifluoroacetic acid, trifluoroacetic anhydride and acetone to obtain a 0.25 mol (with respect to Y) YBCO-TFA solution. The solution was deposited by spin-coating on 5 × 5 mm^2 $LaAlO_3$ (00*l*) (LAO) and $SrTiO_3$ (00*l*) (STO) single crystal substrates (Crystec). The subsequent pyrolysis to remove the organic matter was performed at 310 °C for 30 min in humid, oxidising atmosphere using slow heating and cooling ramps between 3 and 5 °C min^{-1}. It is followed by the growth and sintering process at 810 °C in 200 ppm of O_2 in flowing N_2 gas. For the nucleation stage, the gas is humidified to enable from the reaction of the Ba–Y–F based precursors the growth of YBCO, whereas sintering is performed in dry atmosphere. A detailed description of the chemical reactions taking placed during the pyrolysis and growth process can be found elsewhere.[59,60] The highly epitaxial growth was confirmed and the *c*-axis lattice parameter was determined using a high resolution Discover D8 Bruker diffractometer (X-ray energy = 8.049 keV). Electrical conductivity was measured in Van der Pauw configuration using small excitation currents (±100 μA). The low temperature resistivity, ρ, was measured in a Physical Property Measurement System (PPMS, Quantum Design). Electrical measurements were averaged over two permutations of the electrical contacts and positive and negative excitation currents in DC mode (100 μA). The critical current density was obtained *via* SQUID magnetometry (Quantum Design), as explained elsewhere.[16]

Squared 700 × 700 μm and 100 nm thick Ag electrodes were fabricated in the four corners of the samples to guarantee good contact for electrical measurements using optical lithography (DURHAM) and argon DC sputtering (TSST) at ICMAB's cleanroom facilities. For the Ag decorated YBCO thin films (YBCO|Ag), the same preparation step was used for the fabrication of micro-patterned 30 × 30 μm Ag squares, with a spacing of 20 μm, as shown in Fig. 4(b). The micro-patterning allowed for immediate electrical measurements starting at room temperature (avoiding short circuiting through the continuous Ag layer), whereas at higher temperatures (around 280–300 °C), dewetting of the Ag layer into small islands is observed, see the top panel in Fig. 4(b).

For *in situ* electrical measurements, samples were mounted onto a ceramic sample holder using thin Ag wires glued with high temperature Ag paste onto the top corners, and placed in the centre of a 22 mm tube furnace, equipped with a calibrated thermocouple in close proximity to the sample.

The oxygen exchange activity was studied using electrical conductivity relaxation (ECR) measurements. Therefore, the response of the electrical conductivity, σ, of a thin film to a rapid change in the atmospheric pO_2 is recorded over time and the transient from the initial to the final equilibrium state is analysed to obtain kinetic insight. The modulation of the materials conductivity is caused by changes in the oxygen stoichiometry, c, and thus the charge carrier concentration *via* the oxygen reduction reaction (eqn (1)). Reduction and oxidation processes are triggered by jumps to lower and higher pO_2, respectively. Oxygen partial pressures in the range of 1 mbar to 1 bar were established by mixing high purity gases of O_2 and N_2 using gas flow controllers. All experiments were carried out at atmospheric pressure. Rapid gas atmosphere changes were enabled using high gas flows (0.6l min^{-1}) and automatic valves controlling the switching process *via* a digital relay. After reaching the desired temperature and stabilization for several minutes, the reduction–oxidation cycle was initiated. Thus, each dwell started and ended in pure O_2. Heating and cooling ramps were set between 3 and 10 °C min^{-1} and were always executed in oxygen rich atmosphere.

For thin films, the oxygen diffusion problem can be reduced to 1D, with a linear surface exchange term as boundary condition at the top surface only. In the case that the overall reaction is limited by a surface reaction (*i.e.* $D_{chem} \gg d_{film}k_{chem}$), the solution of Fick's diffusion law for a plane sheet sample geometry can be approximated as:

$$\frac{c(t)-c_\infty}{c_0-c_\infty} \cong \frac{\sigma(t)-\sigma_\infty}{\sigma_0-\sigma_\infty} \cong e^{-\frac{t}{\tau}} \quad (3)$$

with the relaxation time, $\tau = V/(Ak_{chem})$, which relates the characteristic time of the reaction process with the surface

exchange coefficient, k_{chem}, the thin film volume, V, and exposed surface area, A. For the applied model of dense, thin films of rectangular cuboid shape, the ratio V/A reduces to the film thickness, d_{film}, and consequently $\tau = d_{film}/k_{chem}$. The subindices 0 and ∞ indicate the initial and saturation values of the oxygen concentration and the conductivity, respectively. The validity of eqn (3) is limited for small changes in the oxygen stoichiometry and thus small jumps in pO_2, for which a linear correlation with the conductivity can be assumed, *i.e.* $\Delta\sigma \propto \Delta c$ and a simple, linear kinetic regime prevails.[61]

3. Results

3.1. Onset of oxygen incorporation

At elevated temperatures, the $YBa_2Cu_3O_{7-\delta}$ phase is thermodynamically stable only within a narrow (T, pO_2) window. Grown under these conditions, YBCO is highly oxygen deficient, *i.e.* $\delta \gg 0$. Thus, independent of the growth technique, oxygen post-growth treatments are required to reduce the oxygen off-stoichiometry, thereby introducing charge carriers for the superconducting phase to emerge and flourish. To study the initial oxygen uptake of YBCO thin films, the freshly synthesized YBCO material was cooled from the deposition temperature in dry growth atmosphere (pO_2 = 0.2 mbar) without an increase of the pO_2 during the cooling. This results in an oxygen off-stoichiometry of about $\delta \approx 0.5$–0.6, as estimated from the superconducting transition below 40 K (*cf.* Fig. 2(d)).[14] In this strongly reduced state, electrical contacts were fabricated on the top corners for *in situ* resistivity and ECR measurements. Additional batches of samples were prepared with a silver decoration layer of 100 nm on the top surface (YBCO|Ag, see Fig. 4(b)).

The subsequent annealing in 1 atm of oxygen is characterised by a strong chemical driving force for oxygen incorporation. The $\rho(T)$ curves of an aforementioned initial heating in oxygen are shown in Fig. 2(a) for an uncoated and an Ag decorated YBCO sample. The samples exhibit approximately metallic like behaviour with a linear increase of ρ up to a certain temperature, T_{onset}, followed by a strong decrease at higher T. We ascribe the observed drop in resistivity to changes in the charge carrier density due to the onset of noticeable incorporation of oxygen around T_{onset}, as detailed below.

For the bare YBCO sample, the resistivity starts to increase again around 400 °C, due to enhanced thermal scattering. The peak is shifted by approximately 50 °C to lower temperatures for the YBCO|Ag system, as compared to the bare YBCO surface. This effect was observed systematically for the initial oxygenation in all studied samples, with a clear shift of T_{onset} to lower temperatures upon Ag coating, as summarized in Fig. 2(b). Furthermore, the temperature of the maximum in ρ depends on the deployed heating rate, as shown in Fig. 2(c), pointing towards the involvement of kinetic processes.

Similar $\rho(T)$ curves were reported previously for YBCO,[62,63] where it was proposed that this effect is linked to an oxygen ordering mechanism inside the bulk, but the exact origin remained unclear. Based on our findings, we suggest that the maximum in $\rho(T)$ is related to the onset of oxygen incorporation processes and as such a highly relevant indicator for the minimum temperature for an optimised oxygen treatment. The following strong decrease in ρ above approx. 250–320 °C is caused by the increase of the free charge carrier density *via* the oxygen reduction reaction, which is catalytically enhanced through the Ag decoration, as discussed in more detail in the next section. To validate this assumption, we oxygenated bare

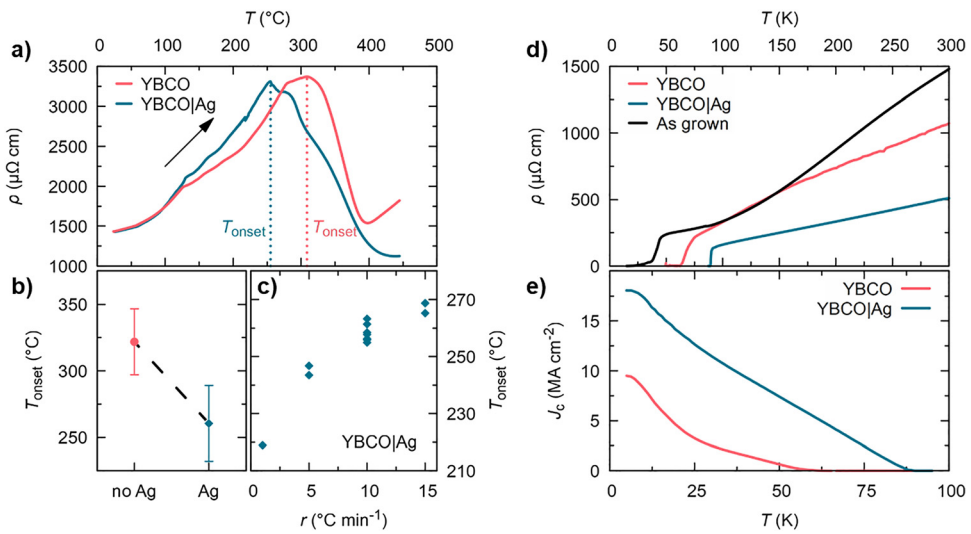

Fig. 2 Investigation of the onset of oxygen incorporation in YBCO thin films using *in situ* resistivity measurements: (a) temperature dependence of ρ for uncoated and Ag decorated YBCO samples during the first heating in oxygen rich atmosphere (1 atm). The maximum in ρ marks the onset temperature for oxygen incorporation, T_{onset}. (b) Onset temperature of oxygen incorporation for bare and Ag decorated YBCO averaged over several samples (at a heating ramp of 10 °C min^{-1}). (c) Dependence of T_{onset} on the heating rate for silver coated samples. (d) Low temperature resistivity and (e) critical current density of bare and Ag coated YBCO oxygenated at 300 °C. Panel (d) additionally shows an as grown YBCO sample without oxygen treatment. Note the absolute temperature scale in (d) and (e).

and Ag coated YBCO for 5 h at 300 °C and analysed the resulting low temperature physical properties. We selected 300 °C, as it approximately lies in between the T_{onset} for bare and Ag coated YBCO.

The low temperature resistivity and critical current density curves are shown in Fig. 2(d) and (e), respectively. The YBCO|Ag specimen exhibits high oxygen doping, characterised by lower resistivity values with high linearity in temperature,[64] a high critical temperature (drop to zero resistance at around 89 K) and comparable J_c values for CSD-TFA grown YBCO samples in our group (J_c of 18 MA cm^{-2} at 5 K and 2 MA cm^{-2} at 77 K).[21,58] On the other hand, the oxygen content in bare YBCO was only slightly enhanced compared to the as grown state, indicated by an increase of the critical temperature from below 40 K to about 64 K and a slightly reduced $\rho(T)$. The low J_c values of the poorly oxygenated bare YBCO sample (9.5 MA cm^{-2} at 5 K and 0 at 77 K) underline the importance of appropriate oxygen doping to achieve excellent superconducting properties. This data is in agreement with our assumption, that the drop in ρ above T_{onset} is linked to the incorporation of oxygen and confirms that silver decoration enables oxygen treatments at reduced temperatures compared to bare YBCO, where kinetic processes and oxygen incorporation are activated at slightly higher temperatures ($T_{onset} \approx 320$ °C).

3.2. Oxygen kinetics of YBCO thin films

In the previous section, we found a low onset temperature of oxygen incorporation of around 300 °C. To determine the oxygen exchange activity of YBCO thin films in a systematic manner, we deployed the ECR technique following two different, time-mirrored protocols, by either starting at high and going to low temperatures (H2L), or in inverse direction going from low to high temperatures (L2H), spanning a temperature range from 375 to 600 °C, with reduction–oxidation cycles every 25 °C. This analysis was performed for bare, as well as silver decorated YBCO thin films.

The temperature and pO_2 profile as well as the evolution of the conductivity for a H2L experiment are presented in Fig. 3(a) and (b). The corresponding $\sigma(T)$ curve is depicted in Fig. 3(c), with the typical spikes for each cycle. Notably, the difference in conductivity between the initial heating and the subsequent cooling steps is small. A kinetic analysis is performed for the isothermal reduction–oxidation steps to obtain surface exchange coefficients. The oxidation transients can be well fitted using to a single exponential decay, as given in eqn (3). An example is shown in Fig. 3(d) and (e), showing the very high fit quality. Generally, reduction processes could not be adequately fit using a single exponential term. The introduction of a second, parallel exponential process, as commonly done in literature,[41,65–67] allows to appropriately model experimental data. As this phenomena was observed for all temperatures, it is unlikely to be an artefact due to the short but non-vanishing furnace flush time.[68] While the necessity for a second relaxation time is possibly related to an intrinsic, material/sample dependent effect, *e.g.* distinct surface areas such as grains and grain boundaries, the exact origin remained unclear within our analysis and is still a controversial topic in literature.[69] For clarity of this manuscript, we restrict the discussion to oxidation processes, sufficiently resembled using a single exponential process.

The obtained surface exchange coefficients for oxidation are shown in Fig. 4(a) for H2L and L2H processes for Ag-free and Ag coated YBCO. We find thermally activated behaviour for all four samples, following Arrhenius-type behaviour with apparent activation energies, E_A. Throughout the analysed temperature range and for both measurement directions, YBCO|Ag exhibits faster kinetics, as compared to bare YBCO. The fact that the simple decoration of the YBCO surface with Ag modifies the oxygen incorporation rate, strongly suggests that the ORR for the studied bare YBCO thin films is limited by surface reactions, as reported previously in our work.[37]

Silver is a well-known catalyst,[70–72] and its efficiency to boost the oxygen reduction and oxygen evolution reaction has been previously demonstrated in literature following different approaches, including the deposition of a thin Ag layer (as performed in our work),[73] using porous Ag current collectors,[74] and *via* core–shell nano-catalysts.[75] Silver can be expected to facilitate the ionization of O_2 by providing easy electron charge transfer to the oxygen molecule and thereby lowering its dissociation energy.[72,76,77] This job sharing mechanism is sketched in Fig. 4(c) and makes the reaction kinetically more favourable, leading to faster exchange coefficients. While we cannot exclude any potential influence of the sample preparation (photolithography, Ag sputtering) on the surface of YBCO, we can exclude that the observed differences between YBCO and YBCO|Ag samples are attributed to it, as both samples were subject to the same procedure (as Ag electrodes were also fabricated on the corners of the bare YBCO samples).

The dotted red line in Fig. 4(a) marks the approximate boundary for the oxygen incorporation being limited by a surface process. It is based on reported values for YBCO diffusion coefficients,[78] *via* $k_{limit} = D_{chem}/d_{film}$. For higher k_{chem} values, bulk diffusion would start co-limiting the exchange process and finally become the governing factor. We note, that also for the silver coated 250 nm thick YBCO films the values fall below k_{limit}. Additionally, oxidation curves of YBCO|Ag can be well modelled using a single saturation time over the full course of the relaxation process, *cf.* Fig. 3(d) and (e), including small times after the change in atmosphere close to $t \approx 0$, which would not be expected for a diffusion (co-)limited process.[61,68] We therefore expect, that all studied samples fall into the surface limited regime, including the ones with catalytic Ag decoration.

Comparing the cooling (H2L) and heating (L2H) processes, one finds a strong dependence for bare YBCO on the direction of the temperature profile, in both magnitude of the observed $k_{chem}(T)$ and apparent activation energies (switching between 0.7 and 3.4 eV), as further discussed at the end of this section. For YBCO|Ag we obtain very similar results at high temperatures for both measurement directions, with reasonably matching k_{chem} values and activation energies of about 1 eV. For the H2L process, we find a second, higher apparent activation energy regime at lower temperatures, with E_A = of 1.8 eV.

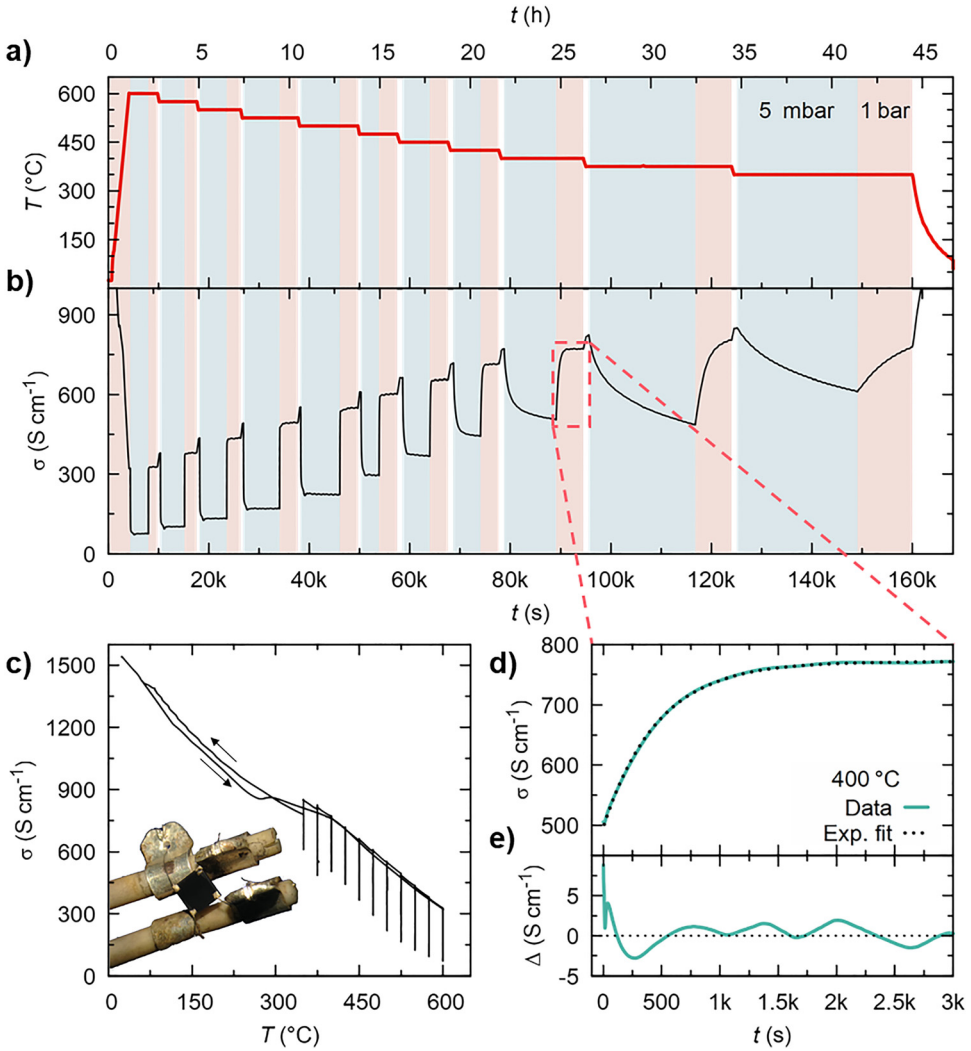

Fig. 3 Electrical conductivity relaxation measurements from high to low (H2L) temperatures for a YBCO|Ag specimen: (a) temperature and (b) conductivity as function of time. Background colouring indicates the oxygen partial pressure (blue: 5 mbar, red: 1 bar, white: 1 bar during heating stages). (c) Conductivity as function of temperature. Note that this sample was cooled in oxygen rich atmosphere after growth and therefore does not exhibit a strong feature around 300 °C, corresponding to the onset of oxygen incorporation. Inset shows optical image of the sample holder. (d) Oxidation step at 400 °C (marked with a rectangular in (b)), fitted using an exponential curve, with the corresponding data-fit deviation in (e).

Interestingly, for pristine YBCO (pink curves with circular symbols) we find a crossing of the trend lines of the surface exchange coefficients for the H2L and L2H measurements. This means that at high temperatures the surface exchange coefficient of the H2L process (starting at high T) is faster compared to the L2H process, while at low temperatures we find the opposite, with L2H possessing faster kinetics. Looking at H2L and L2H processes individually we notice that the relative difference in k_{chem} between silver coated and Ag-free YBCO is smaller at the beginning of the measurements and increases with annealing time. These observations suggest a deactivation of the exchange kinetics of bare YBCO over time. Such a phenomenon is commonly found for similar perovskite oxides, which are frequently used as electrode materials in solid oxide cell applications.[52,53,79]

We studied these deactivation processes qualitatively by performing consecutive isothermal reduction (blue) and oxidation (red) steps at 450 °C, while monitoring the evolution of the conductivity, as shown in Fig. 5(a) and (b) for a fresh set of bare and Ag decorated YBCO samples. Starting from fast relaxation curves, the saturation times for reaching equilibrium drastically increase for uncoated YBCO with increasing total annealing time (indicated by going from light to dark colours), Fig. 5(a). The faster kinetics of the oxidation processes, compared to reduction steps, are primarily a consequence of the higher pO_2 during the forward step. The oxygen pressure is a process parameter for the ORR similarly to the temperature and, thus, higher pO_2 (*i.e.* increased concentration of adsorbate species) or higher T (*i.e.* reactants have higher kinetic energy) result in enhanced chemical activity.

The temporal evolution of the surface exchange coefficient for oxidation is depicted in Fig. 5(c), revealing a strong decrease of almost two orders of magnitude within 17 h of annealing. A very similar degradation rate was observed for YBCO samples

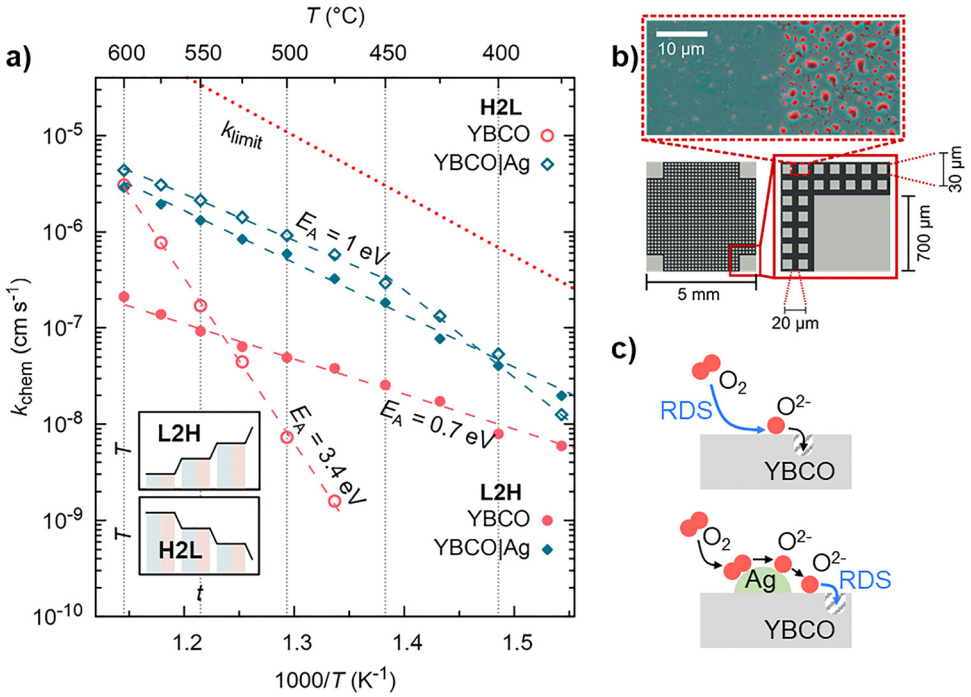

Fig. 4 (a) Arrhenius plot of surface exchange coefficient, k_{chem}, for oxidation steps from 5 to 1000 mbar of Ag-free (pink) and Ag decorated (cyan) CSD-YBCO thin films obtained *via* ECR measurements starting at high temperatures (H2L, open symbols) and low temperatures (L2H, filled symbols). Dashed line correspond to Arrhenius fits for each data set. The insets schematically show the temperature profile and pO_2 steps (blue shaded areas correspond to low, red areas to high pO_2). The red dotted line marks the approximate upper limit for k_{chem} for a surface limited process (see main text). (b) Schematic of the employed micro-patterned Ag coating layer and false color SEM image (combined secondary and back scattered electron mode) showing dewetting of Ag pad into µm-sized islands (above 300 °C). (c) Expected role of the catalytic activity of silver by providing a job sharing mechanism for oxygen incorporation.

grown by pulsed laser deposition, as discussed in the SI1. This strong degradation could not be reverted by thermal treatments at intermediate high temperature (600 °C), as shown in Fig. S1(b).

A small deactivation is also observed for YBCO|Ag, however, at a much lower rate. Silver therefore not only catalytically enhances the oxygen exchange activity of YBCO (compare initial k_{chem} values at 3k s), but also prevents the degradation of its kinetics.

On the other hand, the saturation conductivity values, σ_∞, obtained by raw data fitting, remain approximately constant throughout the measurement for both sample types as well as for oxidation and reduction processes, as shown in Fig. 5(d). This means that the electronic structure is not deteriorated and the thermodynamic saturation value is not modified, opposite to the kinetic oxygen incorporation processes. Note that for bare YBCO sample, saturation was not reached for all reduction transients (within reasonable measurement time), due to the drastically reduced activity. Therefore, the last oxidation steps started from higher oxygen stoichiometries, which would correspond to smaller steps in pO_2 and could slightly affect the extracted k_{chem} values for total annealing times above 30k s. As drastic degradation was observed already before, this does not impact our interpretation.

Based on our observations, we can propose a possible, simplified ORR reaction mechanism, as shown in the reaction energy diagram in Fig. 5(e). In bare YBCO, oxygen incorporation may be limited by either adsorption, ionisation and/or dissociation of O_2, which we can combine in the reaction mechanism, M_1, and leads to the (unknown) oxygen intermediate, {O}. This transition state evolves further to reach the final oxygen bulk level of O^{2-}, possibly *via* additional ionization steps and the recombination with a bulk vacancy and oxygen bulk diffusion, summarized as M_2. As schematically shown in Fig. 5(e), the energy barrier of M_1 is higher than M_2, therefore limiting the overall reaction rate.

As silver coating can be thought to catalytically activate oxygen adsorption, ionisation and/or O_2 dissociation, it provides a faster, alternative pathway, M_{Ag}, running in parallel to M_1 with a strongly reduced energy barrier. In this case, M_2 becomes the rate determining step for the ORR. If this is the case indeed, the observed change in kinetic behaviour going from a bare surface to Ag decoration should be independent of the catalyst concentration (within a certain range). We have tested and confirmed this, using two different Ag layer thicknesses as discussed in the SI2. Given the small film thickness, small k_{chem} values (compared to k_{limit} as shown in Fig. 4(a)), the observed single exponential decay for oxidation steps, and a preliminary analysis of the reaction order of reaction rates[80] (a more thorough analysis is currently in preparation), we anticipate that also for Ag coated YBCO a surface reaction is limiting the overall oxygen incorporation rate. RDS candidates

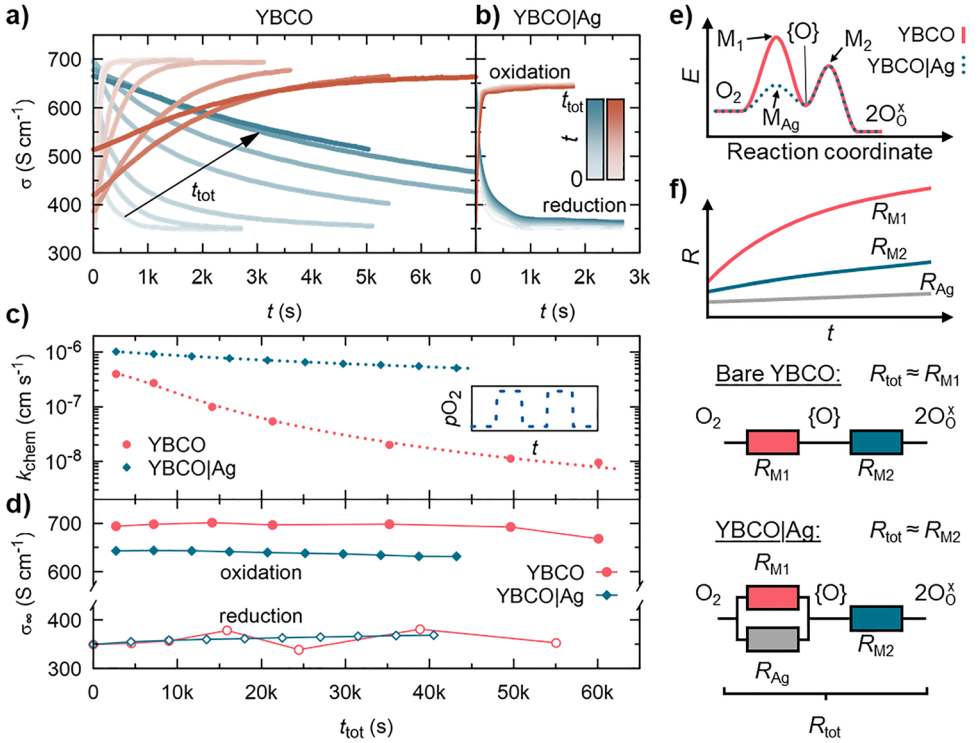

Fig. 5 Consecutive reduction (blue, from bright to dark) and oxidation (red) steps at 450 °C followed using electrical conductivity for (a) uncoated and (b) Ag coated CSD-YBCO. (c) Evolution of the oxidation exchange coefficient, k_{chem}, with the total annealing time at 450 °C, revealing a strong deactivation of the surface activity in bare YBCO. (d) Evolution of the saturation conductivity for oxidation and reduction, obtained by fitting (corresponding to $t = \infty$). (e) Schematic reaction coordinate diagram for bare and Ag decorated YBCO. (f) Electrical analogue of the ORR based on the representation of the elementary mechanisms R_{M_1}, R_{M_2} and R_{Ag} using series and parallel resistances, and a schematic of their evolution with time.

for M_2 include surface diffusion processes of charged oxygen species, (additional) ionization steps or the recombination of an oxygen ion with a bulk oxygen vacancy.

To persuade the reader of the proposed reaction pathway with respect to the observed ageing (*i.e.* the slowing of oxygen exchange activity with time) behaviour, we can qualitatively describe the situation using an electrical resistance analogue, where the different mechanisms are represented by series and parallel resistances, as shown in Fig. 5(f). Bigger resistances correspond to higher energy barriers (and associated slower kinetics). As for bare YBCO $R_{M_1} \gg R_{M_2}$, the total resistance of this reaction is determined by R_{M_1}, and the observed deactivation rate is linked to an increase in magnitude of R_{M_1} with time. In the case of Ag coated YBCO, R_{M_1} is bypassed *via* the small parallel resistance provided *via* the catalytic pathway of silver, R_{Ag}. The total resistance is thus governed by R_{M_2} and our kinetic measurements become sensitive to the degradation rate of R_{M_2}. As the observed deactivation rates strongly differ, we speculate that they are rooted in different chemical and/or structural processes. However, it is highly challenging to identify the specific cause for these degradation mechanisms, as manifold processes down to the atomic level could play a role, including a restructuring of the surface, chemical ageing, the build-up of surface contaminations, *etc.*, and a detailed analysis goes beyond the scope of this work. A future study should be dedicated on potential mechanisms to reverse the described degradation mechanisms, for instance using high temperature treatments under specific oxidising or reducing conditions, or chemical surface treatments, such as etching to restore pristine surface properties.

It becomes clear that the observed temperature dependence of k_{chem} is affected by the ongoing degradation processes, which superimpose an additional time dependence on the measurement. The stronger the degradation rate, the more severe is the deviation from a true Arrhenius behaviour and thus reported activation energies are just apparent ones. Due to ageing, H2L processes lead to larger apparent E_A values, while L2H measurements underestimate it, providing a possible explanation for the strong deviation in observed activation energies for pristine YBCO. The true E_A for bare YBCO is therefore expected to be in-between 0.7 and 3.4 eV, while the value for YBCO|Ag is expected to be around 1 eV, as observed for both measurement directions above 450 °C.

It is noteworthy, that qualitatively similar degradation phenomena were observed in 200 nm thick YBCO thin films grown by pulsed layer deposition,[80] suggesting that ageing phenomena are a more general problem for YBCO surfaces, independent of the synthesis routine. This calls for further detailed studies to provide a clear picture of the origin of these processes.

3.3. Microstructural effects of oxygen treatments

We concluded our experimental work with the bulk analysis using X-ray diffraction of YBCO thin films at two different

stages: as grown and after extended ECR analysis (post ECR). The oxygen content strongly influences the structural parameters, including a tetragonal to orthorhombic phase transition and the shrinkage of the *c*-axis lattice parameter with decreasing oxygen off-stoichiometry. To minimize associated effects, the as grown sample was exposed to an oxygen rich atmosphere during cooling (in contrast to the samples discussed in the previous sections), whereas the oxygen pressure inside the furnace was increased to 1 bar below 600 °C. In Fig. 6(a) we compare the same sample with similar overall oxygen content, but different thermal history, *i.e.* just after the deposition and after extended ECR analysis (post ECR), which was performed between 350 and 600 °C with a total annealing time of about 45 h. First, the data confirms the epitaxial, *c*-axis oriented growth of YBCO on the $SrTiO_3$ single crystal substrate, as we only observe the (00*l*) peak family of $YBa_2Cu_3O_{7-\delta}$ (Y123) in the diffraction pattern. No impurity phases are detected. Second, the annealing does not lead to broad shifts of individual reflections to different angles. However, subtle changes are observed *via* the formation of shoulders and small shifts in 2θ of the Y123 peak family, as magnified in Fig. 6(b) (marked with black arrows). A similar XRD pattern evolution with thermal treatments was obtained for thin YBCO samples grown by pulsed laser deposition (PLD), as shown in Fig. S4.

A commonly found extended structural defect in YBCO is the formation of CuO intergrowths, corresponding to the $YBa_2Cu_4O_{8-\delta}$ (Y124) phase, so called stacking faults (SF). The Y123 stoichiometry is maintained, as the SFs are highly defective including numerous Cu and O vacancies in its vicinity.[84] Due to the second CuO-chain, Y124 has a larger *c*-axis cell parameter and correspondingly its (00*l*) peaks are shifted to lower angles, *cf.* violet bottom markers in Fig. 6(a) and (b). If this defect occurs in alternating stacking with Y123, the $Y_2Ba_4Cu_7O_{15-\delta}$ (Y247) superstructure is formed.[83,85,86]

In agreement with previous reports,[87–90] we do not observe the occurrence of coherent reflections of the Y124 phase. However, the observed shoulders correspond to the Y247 (00*l*) reflections, as can be seen in Fig. 6(b), suggesting the presence of defected regions in the YBCO matrix with an additional second CuO-chain. Furthermore, and as graphically demonstrated in Fig. 6(c), we systematically detected a small 2θ shift of the Y123 peaks after the thermal process (black crosses) towards the closest Y124 reflection (direction indicated with arrows). Note that the pink arrows mark the direction of the closest Y124 peak, not necessarily the one with the same miller indices.

This oscillating positive and negative shift is another hint towards the formation of stacking faults, as confirmed by TEM cross section characterisation, given in Fig. 6(d). We find a high density of additional and extended Y124 intergrowths, easily identified due to their high contrast (marked by arrows). A comparison with a pristine CSD-grown YBCO thin film can be found in Fig. S4(c) and (d). These defects were observed independent of Ag coating and thus are not expected to influence the strong deactivation of the surface kinetics observed exclusively for Ag-free YBCO samples. However, the formation of stacking faults in close proximity to the surface may indeed cause a chemical reconstruction of the surface due to the extra Cu needed for the formation of the Y124 structure, with associated high cationic defect concentrations in its vicinity and further studies on direct and indirect effects of stacking faults on the oxygen kinetics of the material should be attained. Additional, SFs influence the pinning behaviour in the superconducting state, which can be either beneficial or detrimental, depending on their density and length, the

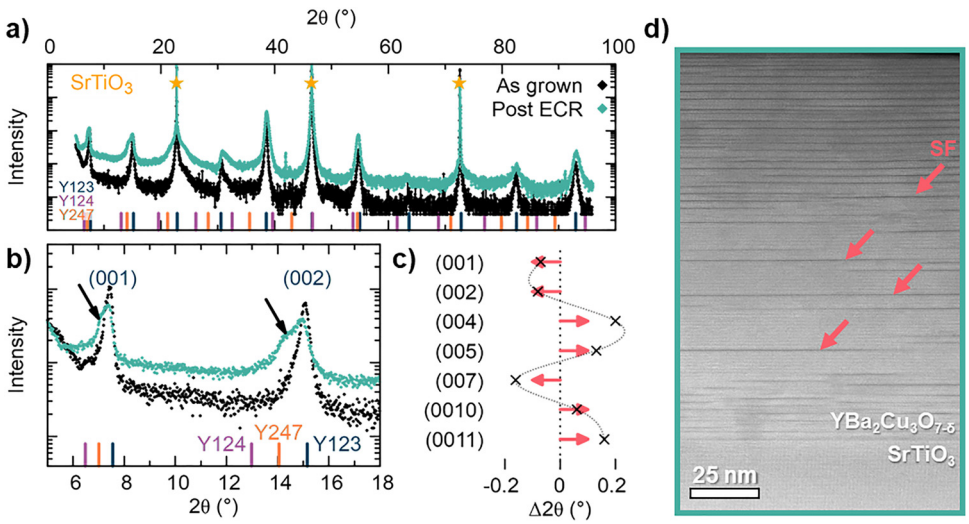

Fig. 6 XRD analysis of as deposited sample and specimen after extended thermal cycling (post ECR). Full range (a) and magnified region (b) of the X-ray diffraction spectra. (00*l*) reference phases for $YBa_2Cu_3O_{7-\delta}$ (Y123),[81] $YBa_2Cu_4O_{8-\delta}$ (Y124),[82] and $Y_2Ba_4Cu_7O_{15-\delta}$ (Y247)[83] are marked at the bottom. Black arrows in (b) indicate the appearance of a shoulder corresponding to the Y247 reflections. (c) Y123 (00*l*) peak shifts in 2θ after annealing compared to as deposited state. The oscillating curve is a guide to the eye. Pink arrows mark the direction of the closest Y124 peak. (d) TEM image of post ECR YBCO sample. Arrows indicate the presence of Y124 intergrowths.

operation temperature and external magnetic field conditions (strength and orientation).[86,89] Therefore, their formation during (long) thermal annealing processes (in oxygen rich environment) has to be taken into account for the optimization of superconducting properties.

4. Conclusions

We analysed the oxygen surface kinetics of YBCO thin films grown by chemical solution deposition using electrical conductivity relaxation measurements. Oxygen incorporation in pristine YBCO was found to be activated already at low temperatures ($\approx$320 °C), however, suffers from rapid degradation. Surface decoration using Ag micro-islands catalyses oxygen surface reactions, shifts its onset to lower temperatures and protects from deactivation *via* an alternative oxygen incorporation pathway based on a job-sharing mechanism. Our findings suggest that oxygen incorporation in all studied thin films is limited by surface reactions and we propose a possible, simplified reaction pathway scenario. Additionally, we observed the formation of extended bulk defects in the form of long CuO stacking faults after extended thermal cycling. It is therefore important to establish a well-designed oxygenation process in terms of temperature and time to allow for good superconducting properties at reduced processing costs and avoid potentially undesired materials degradation processes, highlighting its relevance for both, the academic and industrial superconductivity community.

Author contributions

A. S. developed the original idea of this manuscript and designed the methodology and experimental studies with contributions from T. P. A. S. performed the experimental work, analysed the data and prepared the manuscript. T. P. and A. B. acquired the funding for research and personnel. All authors contributed to the revision of the manuscript.

Conflicts of interest

The authors declare no known conflict of interest.

Data availability

The data that support the findings of this study will be made available upon reasonable request in zenodo at **https://doi.org/10.5281/zenodo.15333534/**.

Supplementary information (SI) is available. See DOI: **https://doi.org/10.1039/d5tc02998h**.

Acknowledgements

This work received government funding managed by the French National Research Agency under France 2030, reference number ''ANR-24-EXSF-0004''. Authors acknowledge funding from EU COST actions OPERA (CA20116) and SUPERQUMAP (CA-21144), the Spanish Ministry of Science and Innovation and the European Regional Development Fund, MCIU/AEI/FEDER for SUPERENERTECH (PID2021-127297OB-C21), ''Severo Ochoa'' Programs for Centers of Excellence in R&D Matrans42 CEX2023-001263-S. They also thank the Catalan Government for 2021 SGR 00440. Authors also thank the Scientific Services at ICMAB and ICN2 Electron Microscopy Division.

References

1 W.-J. Yin, *et al.*, Oxide perovskites, double perovskites and derivatives for electrocatalysis, photocatalysis, and photovoltaics, *Energy Environ. Sci.*, 2019, **12**, 442–462, DOI: **10.1039/C8EE01574K**.

2 A. Pérez-Tomás, A. Mingorance, D. Tanenbaum and M. Lira-Cantú, Metal Oxides in Photovoltaics: All-Oxide, Ferroic, and Perovskite Solar Cells, *The Future of Semiconductor Oxides in Next-Generation Solar Cells*, Elsevier, 2018, pp. 267–356, DOI: **10.1016/B978-0-12-811165-9.00008-9**.

3 M. Acosta, F. Baiutti, A. Tarancón and J. L. MacManus-Driscoll, Nanostructured Materials and Interfaces for Advanced Ionic Electronic Conducting Oxides, *Adv. Mater. Interfaces*, 2019, **6**, 1900462, DOI: **10.1002/admi.201900462**.

4 Y. Chen, *et al.*, A robust and active hybrid catalyst for facile oxygen reduction in solid oxide fuel cells, *Energy Environ. Sci.*, 2017, **10**, 964–971, DOI: **10.1039/c6ee03656b**.

5 A. Molodyk, *et al.*, Development and large volume production of extremely high current density $YBa_2Cu_3O_7$ superconducting wires for fusion, *Sci. Rep.*, 2021, **11**, 1, DOI: **10.1038/s41598-021-81559-z**.

6 M. Eisterer, S. H. Moon and H. C. Freyhardt, Current developments in HTSC coated conductors for applications, *Supercond. Sci. Technol.*, 2016, **29**(6), 060301, DOI: **10.1088/0953-2048/29/6/060301**.

7 J. L. MacManus-Driscoll and S. C. Wimbush, Processing and application of high-temperature superconducting coated conductors, *Nat. Rev. Mater.*, 2021, **6**, 587, DOI: **10.1038/s41578-021-00290-3**.

8 A. Molodyk and D. C. Larbalestier, The prospects of high-temperature superconductors, *Science*, 2023, **380**, 1220–1222, DOI: **10.1126/science.abq4137**.

9 A. Schmid, M. Krammer and J. Fleig, Rechargeable Oxide Ion Batteries Based on Mixed Conducting Oxide Electrodes, *Adv. Energy Mater.*, 2023, **13**, 2203789, DOI: **10.1002/aenm.202203789**.

10 S. Panisset, *et al.*, Exploring the potential of combining over- and under-stoichiometric MIEC materials for oxygen-ion batteries, *J. Power Sources*, 2025, **631**, 236152, DOI: **10.1016/j.jpowsour.2024.236152**.

11 G. F. Harrington, *et al.*, Tailoring Nonstoichiometry and Mixed Ionic Electronic Conductivity in $Pr_{0.1}Ce_{0.9}O_{2-\delta}$/$SrTiO_3$ Heterostructures, *ACS Appl. Mater. Interfaces*, 2019, **11**, 34841–34853, DOI: **10.1021/acsami.9b08864**.

12 D. Chen and H. L. Tuller, Voltage-Controlled Nonstoichiometry in Oxide Thin Films: $Pr_{0.1}Ce_{0.9}O_{2-\delta}$ Case Study, *Adv.*

Funct. Mater., 2014, **24**, 7638–7644, DOI: **10.1002/adfm.201402050**.

13 K. Maas, *et al.*, Tuning Memristivity by Varying the Oxygen Content in a Mixed Ionic–Electronic Conductor, *Adv. Funct. Mater.*, 2020, **30**, 1909942, DOI: **10.1002/adfm.201909942**.

14 J. D. Jorgensen, *et al.*, Structural properties of oxygen-deficient $YBa_2Cu_3O_{7-\delta}$, *Phys. Rev. B: Condens. Matter Mater. Phys.*, 1990, **41**, 1863, DOI: **10.1103/PhysRevB.41.1863**.

15 A. Damascelli, Z. Hussain and Z. X. Shen, Angle-resolved photoemission studies of the cuprate superconductors, *Rev. Mod. Phys.*, 2003, **75**, 473–541, DOI: **10.1103/RevModPhys.75.473**.

16 A. Stangl, A. Palau, G. Deutscher, X. Obradors and T. Puig, Ultra-high critical current densities of superconducting $YBa_2Cu_3O_7\_\delta$ thin films in the overdoped state, *Sci. Rep.*, 2021, **11**, 8176, DOI: **10.1038/s41598-021-87639-4**.

17 P. Cayado, *et al.*, Impact of deoxygenation/reoxygenation processes on the superconducting properties of commercial coated conductors, *Sci. Rep.*, 2023, **13**, 1–13, DOI: **10.1038/s41598-023-44086-7**.

18 T. Prikhna, *et al.*, High Pressure Oxygenation of EuBCO and GdBCO Coated Conductors, *IEEE Trans. Appl. Supercond.*, 2024, **35**, 3–7, DOI: **10.1109/TASC.2024.3511544**.

19 M. Miura, *et al.*, Thermodynamic approach for enhancing superconducting critical current performance, *NPG Asia Mater.*, 2022, **14**, 1–12, DOI: **10.1038/s41427-022-00432-1**.

20 T. Puig, J. Gutierrez and X. Obradors, Impact of high growth rates on the microstructure and vortex pinning of high-temperature superconducting coated conductors, *Nat. Rev. Phys.*, 2023, **6**, 132–148, DOI: **10.1038/s42254-023-00663-3**.

21 X. Obradors, *et al.*, Progress in superconducting $REBa_2Cu_3O_7$ (RE = rare earth) coated conductors derived from fluorinated solutions, *Supercond. Sci. Technol.*, 2024, **37**, 053001, DOI: **10.1088/1361-6668/ad36eb**.

22 D. Chen, *et al.*, Constructing a pathway for mixed ion and electron transfer reactions for O_2 incorporation in $Pr_{0.1}Ce_{0.9}O_{2-x}$, *Nat. Catal.*, 2020, **3**, 116–124, DOI: **10.1038/s41929-019-0401-9**.

23 R. Merkle and J. Maier, How is oxygen incorporated into oxides? A comprehensive kinetic study of a simple solid-state reaction with $SrTiO_3$ as a model material, *Angew. Chem., Int. Ed.*, 2008, **47**, 3874–3894, DOI: **10.1002/anie.200700987**.

24 J. Fleig, G. M. Rupp, A. Nenning and A. Schmid, Towards an Improved Understanding of Electrochemical Oxygen Exchange Reactions on Mixed Conducting Oxides, *ECS Trans.*, 2017, **77**, 93–108, DOI: **10.1149/07710.0093ecst**.

25 A. Stangl, *et al.*, Isotope Exchange Raman Spectroscopy (IERS): A Novel Technique to Probe Physicochemical Processes *In Situ*, *Adv. Mater.*, 2023, **35**, 2303259, DOI: **10.1002/adma.202303259**.

26 A. Stangl, *et al.*, Real-Time Observation of Oxygen Diffusion in CGO Thin Films Using Spatially Resolved Isotope Exchange Raman Spectroscopy, *Small Struct.*, 2024, **5**(11), 2400237, DOI: **10.1002/sstr.202400237**.

27 M. Siebenhofer, *et al.*, Investigating oxygen reduction pathways on pristine SOFC cathode surfaces by: *In situ* PLD impedance spectroscopy, *J. Mater. Chem. A*, 2022, **10**, 2305–2319, DOI: **10.1039/d1ta07128a**.

28 R. Merkle and J. Maier, How is oxygen incorporated into oxides? A comprehensive kinetic study of a simple solid-state reaction with $SrTiO_3$ as a model material, *Angew. Chem., Int. Ed.*, 2008, **47**, 3874–3894, DOI: **10.1002/anie.200700987**.

29 S. J. Rothman, J. L. Routbort, U. Welp and J. E. Baker, Anisotropy of oxygen tracer diffusion in single-crystal $YBa_2Cu_3O_7$-delta, *Phys. Rev. B: Condens. Matter Mater. Phys.*, 1991, **44**, 2326–2333.

30 S. I. Bredikhin, *et al.*, Anisotropy of oxygen self-diffusion in $YBa_2Cu_3O_{7-\delta}$ single crystals, *Phys. C*, 1991, **179**, 286–290, DOI: **10.1016/0921-4534(91)92173-9**.

31 C. Krauns and H. Krebs, Comparison of the oxygen diffusion in $Y1Ba_2Cu_3OY$ bulk materials and thin films, *Z. Phys. B: Condens. Matter*, 1993, **92**, 43–46, DOI: **10.1007/BF01309165**.

32 S. Kittelberger, O. M. Stoll and R. P. Huebener, Oxygen diffusion in thin $YBa_2Cu_3O_7\_\delta$ films studied from isothermal electric resistivity measurements, *Supercond. Sci. Technol.*, 1998, **11**, 744–750, DOI: **10.1088/0953-2048/11/8/006**.

33 H. Jian, *et al.*, Oxygen order control by post-annealing for optimizing critical temperature of YBaCuO coated conductors with silver protective layer, *Phys. C*, 2017, **538**, 40–45, DOI: **10.1016/j.physc.2017.05.007**.

34 L. Li, D. M. Huang, N. Wang, Y. H. Sun and C. Zhou, Diffusion model of oxygen in *c*-axis oriented $YBa_2Cu_3O_7\_\delta$ films, *Phys. C*, 2018, **544**, 1–5, DOI: **10.1016/j.physc.2017.10.016**.

35 J. R. LaGraff and D. A. Payne, Chemical diffusion of oxygen in single-crystal and polycrystalline $YBa_2Cu_3O_{6+x}$ determined by electrical-resistance measurements, *Phys. Rev. B: Condens. Matter Mater. Phys.*, 1993, **47**, 3380–3390, DOI: **10.1103/PhysRevB.47.3380**.

36 T. Motoki, *et al.*, Breakthrough in the reduction of oxygen-annealing time for REBCO melt-textured bulks under an oxygen atmosphere containing water vapor, *Supercond. Sci. Technol.*, 2020, **33**, 034008, DOI: **10.1088/1361-6668/ab6ec2**.

37 P. Cayado, *et al.*, Untangling surface oxygen exchange effects in $YBa_2Cu_3O_{6+x}$ thin films by electrical conductivity relaxation, *Phys. Chem. Chem. Phys.*, 2017, **19**, 14129–14140, DOI: **10.1039/c7cp01855j**.

38 J. Shi, M. Martens, F. Ludwig, K. Dilger and K. D. Becker, Optical absorption and redox kinetics of YBa2Cu3O7 - δthin films studied by optical in-situ spectroscopy, *Solid State Ionics*, 2018, **315**, 98–101, DOI: **10.1016/j.ssi.2017.12.002**.

39 A. Schmid, G. M. Rupp and J. Fleig, How to Get Mechanistic Information from Partial Pressure-Dependent Current-Voltage Measurements of Oxygen Exchange on Mixed Conducting Electrodes, *Chem. Mater.*, 2018, **30**, 4242–4252, DOI: **10.1021/acs.chemmater.8b00597**.

40 R. Merkle and J. Maier, Oxygen incorporation into Fe-doped $SrTiO_3$: Mechanistic interpretation of the surface reaction, *Phys. Chem. Chem. Phys.*, 2002, **4**, 4140–4148, DOI: **10.1039/b204032h**.

41 A. Stangl, *et al.*, Tailored nano-columnar La_2NiO_4 cathodes for improved electrode performance, *J. Mater. Chem. A*, 2022, **10**, 2528, DOI: 10.1039/d1ta09110g.
42 S. Miyoshi, A. Takeshita, S. Okada and S. Yamaguchi, Rate-determining elementary step of oxygen reduction reaction at (La,Sr)CoO_3-based cathode surface, *Solid State Ionics*, 2016, **285**, 202–208, DOI: 10.1016/j.ssi.2015.08.015.
43 L. Wang, R. Merkle, Y. A. Mastrikov, E. A. Kotomin and J. Maier, Oxygen exchange kinetics on solid oxide fuel cell cathode materials-general trends and their mechanistic interpretation, *J. Mater. Res.*, 2012, **27**, 2000–2008, DOI: 10.1557/jmr.2012.186.
44 M. Mosleh, M. Sogaard and P. V. Hendriksen, Kinetics and Mechanisms of Oxygen Surface Exchange on $La_{0.6}Sr_{0.4}FeO_{3-\delta}$ Thin Films, *J. Electrochem. Soc.*, 2009, **156**, B441, DOI: 10.1149/1.3062941.
45 S. Tsukui, *et al.*, Oxygen and cation diffusion in YBCO coated conductors, *Phys. C*, 2003, **392–396**, 841–846, DOI: 10.1016/S0921-4534(03)01132-8.
46 H. Behner, K. Rührnschopf, G. Wedler and W. Rauch, Surface reactions and long time stability of YBCO thin films, *Phys. C*, 1993, **208**, 419–424, DOI: 10.1016/0921-4534(93)90216-D.
47 M. Caldararu, A. Ovenston and J. R. Walls, The electrical and catalytic properties of $YBa_2Cu_3O_{7-x}$ for oxidation reactions below 400 °C, *J. Mater. Sci.*, 1997, **32**, 2895, DOI: 10.1023/A:1018628618206.
48 P. Cayado, *et al.*, Determination of the Oxygen Chain Ordering in $REBa_2Cu_3O_{7-\delta}$ by Electrical Conductivity Relaxation Measurements, *ACS Appl. Electron. Mater.*, 2021, **3**, 5374–5382, DOI: 10.1021/acsaelm.1c00861.
49 J. Shimoyama, S. Horii, K. Otzschi and K. Kishio, How to Optimize Critical Current Performance of RE123 Materials by Controlling Oxygen Content, *MRS Proc.*, 2001, **689**, E8.18, DOI: 10.1557/PROC-689-E8.18.
50 P. Schleger, W. N. Hardy and B. X. Yang, Thermodynamics of oxygen in $Y_1Ba_2Cu_3O_x$ between 450 °C and 650 °C, *Phys. C*, 1991, **176**, 261–273, DOI: 10.1016/0921-4534(91)90722-B.
51 J. Chen, *et al.*, Significant improvement of the critical current of MOD-derived $YBa_2Cu_3O_{7-\delta}$-coated conductors by post-annealing treatment, *Appl. Phys. Express*, 2021, **14**, 055506, DOI: 10.35848/1882-0786/abf4f0.
52 S. J. Benson, Degradation of $La_{0.6}Sr_{0.4}Fe_{0.8}Co_{0.2}O_{3-\delta}$ in Carbon Dioxide and Water Atmospheres, *J. Electrochem. Soc.*, 1999, **146**, 1305, DOI: 10.1149/1.1391762.
53 A. Egger, N. Schrödl, C. Gspan and W. Sitte, $La_2NiO_{4+\delta}$ as electrode material for solid oxide fuel cells and electrolyzer cells, *Solid State Ionics*, 2017, **299**, 18–25, DOI: 10.1016/j.ssi.2016.10.002.
54 Đ. Tripković, *et al.*, Thermally Controlled Activation and Passivation of Surface Chemistry and Oxygen-Exchange Kinetics on a Perovskite Oxide, *Chem. Mater.*, 2022, **34**, 1722, DOI: 10.1021/acs.chemmater.1c03901.
55 X. Tong, *et al.*, Performance and stability of Ruddlesden-Popper $La_2NiO_{4+\delta}$ oxygen electrodes under solid oxide electrolysis cell operation conditions, *Ceram. Int.*, 2017, **43**, 10927–10933, DOI: 10.1016/j.ceramint.2017.05.130.
56 S. B. Adler, Factors governing oxygen reduction in solid oxide fuel cell cathodes, *Chem. Rev.*, 2004, **104**, 4791–4843, DOI: 10.1021/cr020724o.
57 M. Bonura, P. Cayado, K. Konstantopoulou, M. Alessandrini and C. Senatore, Heating-Induced Performance Degradation of $REBa_2Cu_3O_{7-x}$ Coated Conductors: An Oxygen Out-Diffusion Scenario with Two Activation Energies, *ACS Appl. Electron. Mater.*, 2022, **4**, 1318–1326, DOI: 10.1021/acsaelm.2c00065.
58 X. Obradors, *et al.*, Progress towards all-chemical superconducting $YBa_2Cu_3O_7$-coated conductors, *Supercond. Sci. Technol.*, 2006, **19**(3), S13–S26, DOI: 10.1088/0953-2048/19/3/003.
59 C. F. Sánchez-Valdés, T. Puig and X. Obradors, *In situ* study through electrical resistance of growth rate of trifluoroacetate-based solution-derived $YBa_2Cu_3O_7$ films, *Supercond. Sci. Technol.*, 2015, **28**, 024006, DOI: 10.1088/0953-2048/28/2/024006.
60 X. Obradors, *et al.*, Growth, nanostructure and vortex pinning in superconducting $YBa_2Cu_3O_7$ thin films based on trifluoroacetate solutions, *Supercond. Sci. Technol.*, 2012, **25**, 123001, DOI: 10.1088/0953-2048/25/12/123001.
61 A. Stangl, Electrical conductivity relaxation (ECR) measurements: considerations and validation for thin films, 2025, in preparation.
62 K. Hauser, S. Kittelberger, R. P. Huebener, E. Haufe and T. Schwellinger, Oxygen mobility and charge transport in $YBa_2Cu_3O_{7-}\delta$, *J. Low Temp. Phys.*, 1996, **105**, 1409–1414, DOI: 10.1007/BF00753897.
63 O. B. Anikeeva, A. I. Romanenko and L. P. Kozeeva, Effect of Oxygen Redistribution on the Normal and Superconducting Properties of Yttrium High-Temperature Superconductors, *J. Struct. Chem.*, 2003, **44**, 227–230, DOI: 10.1023/A:1025546707371.
64 H. Castro and G. Deutscher, Anomalous Fermi liquid behavior of overdoped high-Tc superconductors, *Phys. Rev. B: Condens. Matter Mater. Phys.*, 2004, **70**, 1–8, DOI: 10.1103/PhysRevB.70.174511.
65 C. Ling, C. L. Chen and A. J. Jacobson, Electrical conductivity relaxation studies of oxygen transport in epitaxial $YBa_2Cu_3O_{7-\delta}$/thin films, *IEEE Trans. Appl. Supercond.*, 2003, **13**, 2882–2885, DOI: 10.1109/TASC.2003.812032.
66 L. Yan, B. Kavaipatti, K.-C. Chang, H. You and P. Salvador, Microstructural Effects on the Oxygen Exchange Kinetics of $La_{0.7}Sr_{0.3}MnO_3$ Thin Films, *ECS Trans.*, 2019, **35**, 2063–2075, DOI: 10.1149/1.3570197.
67 G. Kim, S. Wang, A. J. Jacobson and C. L. Chen, Measurement of oxygen transport kinetics in epitaxial $La_2NiO_{4+\delta}$ thin films by electrical conductivity relaxation, *Solid State Ionics*, 2006, **177**, 1461–1467, DOI: 10.1016/j.ssi.2006.07.013.
68 M. W. den Otter, H. J. M. Bouwmeester, B. A. Boukamp and H. Verweij, Reactor Flush Time Correction in Relaxation Experiments, *J. Electrochem. Soc.*, 2001, **148**, J1, DOI: 10.1149/1.1337604.
69 Z. Shen, *et al.*, Universal *In Situ* Isotope Exchange Raman Spectroscopy (IERS) Methodology for Measuring Oxygen

Surface Exchange Dynamics Using a Probe Layer, *Adv. Funct. Mater.*, 2025, in press.

70 C. Rehren, M. Muhler, X. Bao, R. Schlögl and G. Ertl, The Interaction of Silver with Oxygen, *Z. Phys. Chem.*, 1991, **174**, 11–52, DOI: **10.1524/zpch.1991.174.part_1.011**.

71 W. X. Li, C. Stampfl and M. Scheffler, Why is a Noble Metal Catalytically Active? The Role of the O–Ag Interaction in the Function of Silver as an Oxidation Catalyst, *Phys. Rev. Lett.*, 2003, **90**, 4, DOI: **10.1103/PhysRevLett.90.256102**.

72 R. Merkle and J. Maier, The significance of defect chemistry for the rate of gas-solid reactions: Three examples, *Top. Catal.*, 2006, **38**, 141–145, DOI: **10.1007/s11244-006-0079-5**.

73 A. Egger and W. Sitte, Enhanced oxygen surface exchange of $La_2NiO_{4+\delta}$ by means of a thin surface layer of silver, *Solid State Ionics*, 2014, **258**, 30–37, DOI: **10.1016/j.ssi.2014.01.038**.

74 T. T. Wan, *et al.*, Performance variability of $Ba_{0.5}Sr_{0.5}Co_{0.8}Fe_{0.2}O_{3-\delta}$ cathode on proton-conducting electrolyte SOFCs with Ag and Au current collectors, *Rare Met.*, 2018, **37**, 633–641, DOI: **10.1007/s12598-017-0942-5**.

75 X. Ding, X. Zhao, Y. Yan and M. Li, Enhancing oxygen reduction activity of perovskite cathode decorated with core@shell nano catalysts, *Int. J. Hydrogen Energy*, 2019, **44**, 22122–22128, DOI: **10.1016/j.ijhydene.2019.06.122**.

76 C.-L. Chang, T.-C. Lee and T.-J. Huang, Oxygen reduction mechanism and performance of $Y_1Ba_2Cu_3O7$-d as a cathode material in a high-temperature solid-oxide fuel cell, *J. Solid State Electrochem.*, 1998, **2**, 291–298, DOI: **10.1007/s100080050103**.

77 G. I. Golodets, *et al.*, The Dissociation of Molecular Oxygen, The Recombination of Oxygen Atoms and Isotopic Exchange with Molecular Oxygen, in *Studies in Surface Science and Catalysis*, ed. G. I. Golodets, Elsevier, 1983, ch. VII, vol. 15, pp. 180–199, DOI: **10.1016/S0167-2991(08)64832-6**.

78 M. D. Vázquez-Navarro, A. Kursumovic and J. E. Evetts, Study and modelling of oxygen diffusion in $YBa_2Cu_3O_7$-delta under isothermal conditions, *Supercond. Sci. Technol.*, 1999, **12**, 1117–1122, DOI: **10.1088/0953-2048/12/12/320**.

79 D. Kim, J. W. Park, B.-H. Yun, J. H. Park and K. T. Lee, Correlation of Time-Dependent Oxygen Surface Exchange Kinetics with Surface Chemistry of $La_{0.6}Sr_{0.4}Co_{0.2}Fe0.8O_{3-\delta}$ Catalysts, *ACS Appl. Mater. Interfaces*, 2019, **11**, 31786–31792, DOI: **10.1021/acsami.9b06569**.

80 A. Stangl, *Oxygen kinetics and charge doping for high critical current YBCO films*, Universitat Autònoma de Barcelona, 2019, ISBN: 9788449087103, **https://hdl.handle.net/10803/667212**.

81 A. Williams, G. H. Kwei, R. B. Von Dreele, I. D. Raistrick and D. L. Bish, Joint x-ray and neutron refinement of the structure of superconducting $YBa_2Cu_3O_{7-x}$: Precision structure, anisotropic thermal parameters, strain, and cation disorder, *Phys. Rev. B: Condens. Matter Mater. Phys.*, 1988, **37**, 7960–7962, DOI: **10.1103/PhysRevB.37.7960**.

82 H. Hara, *et al.*, Fabrication of a superconducting $YBa_2Cu_4O_8$ film via coprecipitation, *Jpn. J. Appl. Phys.*, 2019, **58**, 28–31, DOI: **10.7567/1347-4065/ab2866**.

83 D. E. Morris, *et al.*, Synthesis and properties of the 2:4:7 superconductors $R_2Ba_4Cu_7O_{15-x}$ (R = Y, Eu, Gd, Dy, Ho, Er), *Phys. Rev. B: Condens. Matter Mater. Phys.*, 1989, **40**, 11406–11409, DOI: **10.1103/PhysRevB.40.11406**.

84 J. Gazquez, *et al.*, Emerging diluted ferromagnetism in high-Tc superconductors driven by point defect clusters, *Adv. Sci.*, 2015, **3**, 1–8, DOI: **10.1002/advs.201500295**.

85 J. Díez-Sierra, *et al.*, High Critical Current Density and Enhanced Pinning in Superconducting Films of $YBa_2Cu_3O_{7-}\delta$ Nanocomposites with Embedded $BaZrO_3$, $BaHfO_3$, $BaTiO_3$, and $SrZrO_3$ Nanocrystals, *ACS Appl. Nano Mater.*, 2020, **3**, 5542–5553, DOI: **10.1021/acsanm.0c00814**.

86 J. Chen, *et al.*, Significant improvement of the critical current of MOD-derived $YBa_2Cu_3O_{7-}\delta$-coated conductors by post-annealing treatment, *Appl. Phys. Express*, 2021, **14**, 055506, DOI: **10.35848/1882-0786/abf4f0**.

87 S. H. Wee, *et al.*, Formation of stacking faults and their correlation with flux pinning and critical current density in Sm-doped $YBa_2Cu_3O_{7-\delta}$ films, *Phys. Rev. B: Condens. Matter Mater. Phys.*, 2011, **83**, 1–6, DOI: **10.1103/PhysRevB.83.224520**.

88 E. D. Specht, *et al.*, Stacking faults in $YBa_2Cu_3O_{7-x}$: Measurement using X-ray diffraction and effects on critical current, *Appl. Phys. Lett.*, 2006, **89**, 87–90, DOI: **10.1063/1.2364185**.

89 A. H. Puichaud, S. C. Wimbush and R. Knibbe, Enhanced low-temperature critical current by reduction of stacking faults in REBCO coated conductors, *Supercond. Sci. Technol.*, 2017, **30**, 074005, DOI: **10.1088/1361-6668/aa6ce8**.

90 E. F. Talantsev, *et al.*, Hole doping dependence of critical current density in $YBa_2Cu_3O_{7-}\delta$ conductors, *Appl. Phys. Lett.*, 2014, **104**, 242601, DOI: **10.1063/1.4883483**.

91 J. Claus, G. Borchardt, S. Weber and S. Scherrer, Oxygen Diffusion and Surface Exchange Kinetics in YBa2Cu3O6+x, *Z. Phys. Chem.*, 1998, **206**, 49–71, DOI: **10.1524/zpch.1998.206.Part_1_2.049**.